Many-body Szilárd engine with giant number fluctuations

Omer Chor,[1] Amir Sohachi,[1] Rémi Goerlich,[2] Eran Rosen,[2] Saar Rahav,[3,*] and Yael Roichman[1,2,†]

[1]*Raymond & Beverly Sackler School of Physics and Astronomy, Tel Aviv University, Tel Aviv 6997801, Israel*

[2]*Raymond & Beverly Sackler School of Chemistry, Tel Aviv University, Tel Aviv 6997801, Israel*

[3]*Schulich Faculty of Chemistry, Technion–Israel Institute of Technology, Haifa 3200008, Israel*

(Received 23 November 2022; revised 21 August 2023; accepted 25 October 2023; published 1 December 2023)

Szilárd's information engine is a canonical example in the field of thermodynamics of information. We realize experimentally a macroscopic many-particle Szilárd engine that consists of active particles and use it to lift a mass against gravity. We show that the extractable work per cycle increases when the raised weight is changed more gradually during the process. Interestingly, we find that the ideal extractable work grows with the number of particles due to giant number fluctuations. This is in contrast to the calculated behavior of a similar engine operating on thermal particles.

DOI: 10.1103/PhysRevResearch.5.043193

I. INTRODUCTION

In recent years there has been a renewed interest in the connection between information and thermodynamics [1–10]. This fundamental line of research, originating with Maxwell's celebrated thought experiment [11] is now a reality, having been experimentally tested in various settings [12–24]. The first illustration of how a Maxwell's demon can be used to construct an engine is due to Szilárd [25], who proposed a single-molecule engine directly converting information to work [Fig. 1(a)].

In Szilárd's engine, an ideal gas molecule is placed in a rectangular box that is in equilibrium with a surrounding heat bath. A mobile partition is then placed in the center of the box, and a measurement is made to determine which side the molecule occupies. The information gained by the measurement $I = \ln 2$ is proportional to the reduction in entropy of the system. Next, the single-molecule gas is allowed to expand isothermally, performing work of $W = k_B T \ln 2$. The partition is then removed, bringing the system to its original state. As in any typical engine, this process is repeated in a cyclic manner.

While previous experimental realizations have mainly focused on single-particle systems, theoretical analyses have also explored generalizations to many-body information engines [26–32]. In a classical many-body Szilárd's engine [26] [Fig. 1(b)], N ideal-gas particles are placed in the box, and the measurement determines the number of particles in each side: N_L, N_R (for simplicity, an odd $N = N_L + N_R$ is assumed). Work is extracted from the system by taking advantage of the pressure difference between the two halves. In the many-body case, work extraction increases with the imbalance in the initial division of particles. This is the case for any system where the pressure is a monotonic function of the density (see Appendix A).

Information engines are inherently out-of-equilibrium due to the application of measurement outcome-dependent feedback. In most of the literature, this is the sole mechanism that drives the engine away from equilibrium. Only very recently, connection to a nonequilibrium environment [33,34], or an active working substance [35], were considered.

Here, we consider a Szilárd engine operating on a many-body active system. In a Szilárd engine operating on an ideal gas, the number of particles in each half is distributed binomially, due to thermally induced number (or density) fluctuations. In contrast, if the engine operated instead on a system that exhibits giant number fluctuations, the imbalance between both halves would be more prominent. Giant number fluctuations are known to exist in driven dissipative systems [36–38] and active matter [39–45]. Therefore, realizations with large number differences $|N_L - N_R|$ are more likely to occur in a Szilárd engine with active particles. This, in turn, should result in a higher amount of extractable work.

II. EXPERIMENTAL SETUP

In the following, we describe our experimental realization of a many-body Szilard engine consisting of self-propelled particles [Fig. 1(c)] (see Supplemental Material (SM) Movie 1 [46]). We start by characterizing the properties of the active system, focusing on the distribution of N_R, and on the dependence of the pressure on the number of particles. We investigate the consequence of increasing the number of particles and verify that the giant number fluctuations result in an increase of the extractable work, in contrast to an ideal-gas many-body Szilárd engine. Finally, we experimentally extract work from the Szilárd engine by lifting a mass against gravity. We compare the measured work to the expected work within the constraints of the protocol, and to the work extractable in an optimal (quasistatic) process.

*rahavs@ch.technion.ac.il

†roichman@tauex.tau.ac.il

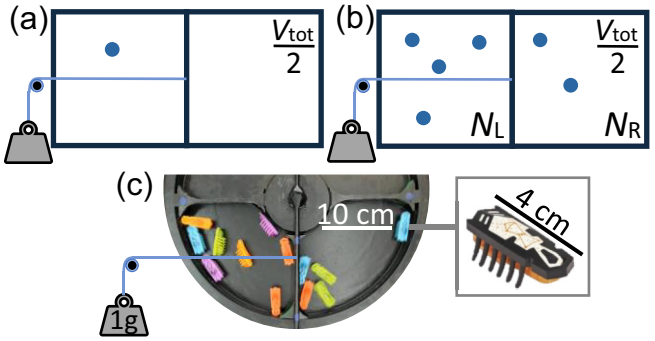

FIG. 1. (a) Szilárd's engine. (b) Many-body generalization. (c) Our experimental setup with many active particles. The arena is round and the partition is free to rotate on an axle placed in its center. A mass is attached to a string that is connected to the partition, converting the circular motion of the partition to vertical motion and pulling the mass against gravity (hence extracting work).

Particles in our system are self-propelled, elongated bristle robots (Hexbug, Nano). Each robot has 12 flexible legs on which it jumps due to the rotation of an internal, battery-powered motor [47]. Bristle robots (bbots) exhibit typical active matter behaviors such as clustering [47–49]. The motion of a single bbot can be described as directed random motion with a persistence length of more than 1 m [50], which is larger than the radius of our system, $R \simeq 0.2$ m. Bbots exhibit a slightly chiral motion that did not significantly affect the resulting pressure and particle distribution. We place the bbots in a half-circular arena with rounded edges to prevent particles from getting stuck in corners. The arena has a detachable partition that can be inserted at will and rotates freely on an axle. We record the experiments with a web camera (Logitech, Brio 4K).

III. RESULTS

Pressure as a function of density. The relation between pressure and density is determined by measuring the average steady-state volume occupied by the bbots under a specified external pressure. A constant force is applied by attaching a mass m to the partition. The bbots are positioned on one side of the partition and exert pressure to counteract the gravitational force (see SM Movie 2 [46]). The mechanical quasi-two-dimensional pressure that the bbots apply on the partition is given by mg/L, where g is the gravitational acceleration, and L is the length of the partition. The density, at this pressure, is given by the number of bbots in the chamber divided by the average volume they occupy.

In Fig. 2, we plot the applied pressure as a function of the average measured density N/V, demonstrating that pressure is a monotonous function that grows with density. Since a linear dependence of the pressure on density is observed throughout the density range tested in our experiment, we fit the pressure to an ideal-gaslike equation of state $P = \alpha N/V + P_0$, with a fitting parameter $\alpha = (1.78 \pm 0.21) \times 10^{-4}$ J (Fig. 2, solid line). The nonzero intercept $P_0 = (2.18 \pm 0.52) \times 10^{-2}$ N/m is attributed to a combination of static friction and the finite size of the system. At high loads, the finite system size restricts the partition and volume fluctuations, truncating its

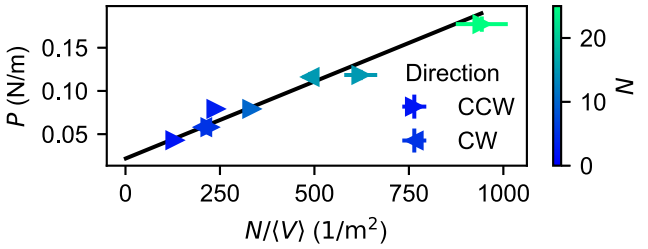

FIG. 2. Applied pressure as a function of density. A linear fit $P = \alpha N/V + P_0$ is shown in a black line. Different colors indicate different particle numbers N. To rule out a possible effect of the chiral motion of bbots, measurements were made with particles at either side of the partition (triangular symbols indicate the direction of applied force on the partition).

range. This leads to an underestimation of the mechanical equilibrium volume and an overestimation of the pressure in a nontrivial manner (see Appendix B). It should be noted that the intercept is canceled out in subsequent calculations that are based on the difference of pressures from both sides.

The dependence of pressure on particle number may cease to be linear at higher densities. Nonetheless, active particles were previously shown to have a monotonic dependence of pressure on density if their Péclet number is high enough [51,52]. The tendency of active particles to cluster near walls [51] can contribute to the forces they apply on them, which can help maintain high pressures even when large clusters form. A theoretical analysis of the pressure and number fluctuations at high densities is beyond the scope of the current work.

Number fluctuations. We use image analysis [53] to measure the distribution of the number of particles in each half, e.g., $\Pr(N_R)$. For small N the distribution is essentially that of ideal thermal particles [Fig. 3(a)]. In contrast, much wider distributions are observed for larger N_R [Fig. 3(b)]. In Fig. 3(c), we show the standard deviation ΔN_R of N_R for different values of N. The results exhibit a transition from $\Delta N_R \propto \sqrt{N}$

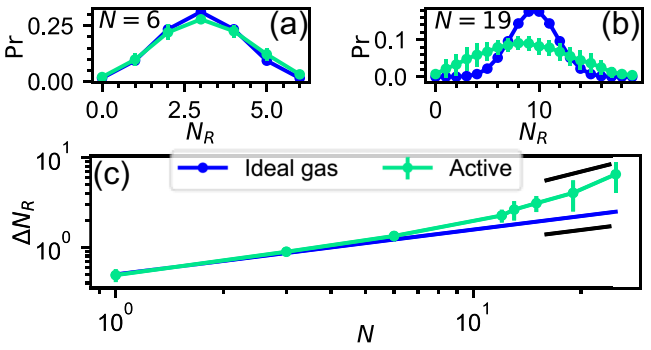

FIG. 3. Experimental measurement of number fluctuations. (a)–(b) Histograms of the number of particles in the right half of the system N_R for $N = 6, 19$ particles (green line), respectively, compared to the expected distribution for an ideal gas (blue line). (c) The standard deviation of the distribution of the number of particles in the right half of the system ΔN_R as a function of N. The black lines are the power laws for a system in equilibrium ($\Delta N_R \sim N^{1/2}$, bottom) and for a system with giant number fluctuations ($\Delta N_R \sim N$, top). We observe a transition between these regimes when the number of particles is increased.

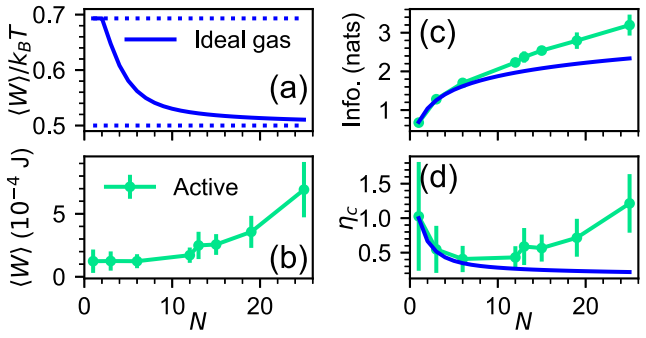

FIG. 4. Upper bound on mean work per cycle as a function of the number of particles for the many-body Szilárd's engines: (a) passive (solid blue line) and (b) active (green points). Values for the ideal gas are normalized by k_BT whereas, for the active gas, work is in units of 10^{-4} Joules. (c) Information per measurement as a function of N. (d) The efficiency of converting information to work, for quasistatic work extraction, as a function of N.

towards the maximally possible exponent $\Delta N_R \propto N$. Such high number fluctuations were found for other rodlike active materials [39–42].

Maximal extractable work. Keeping in mind Szilárd's original view, we consider a case where work is extracted by connecting a mass that is lifted against gravity. The work $W = \int F dh$ clearly depends on both the time-dependent height h of the mass and the force F applied at every instant. In equilibrium, optimal work extraction is achieved by following a quasistatic process in which the force balances the pressure difference at any time. In this case, all the free energy difference is converted into work. This quasistatic work is given by

$$W(k) = \int_{\frac{1}{2}V_{tot}}^{\frac{N/2+k}{N}V_{tot}} P_R dV_R + \int_{\frac{1}{2}V_{tot}}^{\frac{N/2-k}{N}V_{tot}} P_L dV_L, \qquad (1)$$

where $k = N_R - N/2$ and $P_{L,R}$ are the pressure of the left/right-hand side of the system. For an ideal gas

$$W(k) = Nk_BT\left(\frac{1}{2}\ln\left(1-4\left(\frac{k}{N}\right)^2\right) + \frac{k}{N}\ln\frac{1+2\frac{k}{N}}{1-2\frac{k}{N}}\right), \qquad (2)$$

where T is the temperature and k_B is Boltzmann's constant. The average extracted work, given that particles are noninteracting and their spatial distributions are uniform, is $\langle W\rangle = \sum_{k=-N/2}^{N/2} W(k)\Pr(k)$, with $\Pr(k) = (\frac{1}{2})^N\binom{N}{\frac{N}{2}+k}$. For an engine operating on an ideal gas and $N \gg 1$, the mean work can be approximated by noting that $\Pr(k)$ is a fast-decaying function as $|k/N|$ grows. As a result one can expand $W(k)$ [26]:

$$W(k) = Nk_BT\left(2\left(\frac{k}{N}\right)^2 + O\left(\left(\frac{k}{N}\right)^4\right)\right), \qquad (3)$$

$$\lim_{N\to\infty}\langle W\rangle = \frac{2k_BT}{N}\langle k^2\rangle = \frac{1}{2}k_BT, \qquad (4)$$

and higher-order terms vanish. Therefore, the mean extractable work depends on number fluctuations ($\langle k^2\rangle = (\Delta N_R)^2$), and for an ideal-gas-based Szilárd engine it transitions from $k_BT\ln 2$ to $k_BT/2$ as N increases [Fig. 4(a)].

We calculate $\langle W\rangle$ for the active particle system following the same analysis, substituting α (Fig. 2) for k_BT and the experimentally measured distribution $\Pr(k)$ in place of the binomial distribution [Fig. 4(b)]. We find that the calculated $\langle W\rangle$ increases with N. This is a clear qualitative difference between information engines operating on active and thermal particles.

Information and efficiency. The protocol used to extract work uses information about the number of particles in each half to determine the weight that can be lifted. The information measure that fits this protocol is the Shannon information of the distribution $\Pr(N_R)$: $I = -\sum_{N_R=0}^{N}\Pr(N_R)\ln\Pr(N_R)$. For an engine with thermal particles, the efficiency of converting information to work is $\eta_c = \langle W\rangle/k_BTI$. For comparison, we use a figure of merit $\eta_c = \langle W\rangle/\alpha I$ also for our active information engine.

The information and η_c for both cases are shown in Figs. 4(c) and 4(d). The wider number distribution of the active particles is reflected in larger I. At the same time, the calculated η_c for the active particles is larger than for their thermal counterparts, especially for large N. In fact, $\eta_c > 1$ is found for the active system with $N = 25$. It should be stressed that in the active system, there is an additional source of energy that is not taken into account in the definition of η_c, which is therefore not the true thermodynamic efficiency of the setup.

Experimental work extraction. In theoretical analyses of information engines, work is commonly assumed to be extracted in an optimal way and more attention is directed to finding the optimal measurement protocol [27,28,54]. Extraction of the full amount of energy from the post-measurement state is an experimental challenge, requiring the ability to control the system quasistatically [14–16]. In many cases, a slow quasistatic work extraction process is undesired and impractical, as is in our experimental setup which has long relaxation times and is controlled manually. Taking these considerations into account, we demonstrate that measurable work can be extracted from our system by testing a finite-time approximation of the optimal protocol [55].

Work extraction is demonstrated using the following protocol. The partition is placed in the center of the arena, with different numbers of bbots on its sides, thereby matching a particular measurement of N_L, N_R. A string with three weights is then attached to the partition. The weights are chosen so their sum partially balances the expected pressure imbalance. The partition is then allowed to move freely so that after a while it fluctuates around the volume ratio where the forces on it are balanced. At this point, the lower weight (m_1) is removed by burning the string connecting it to the other weights (see SM Movie 3 [46]). The lower net weight on the string means that the partition is free to move and fluctuate around a new balancing point while raising the remaining weights. The process is repeated. At the end of the process, the ith weight has been raised by Δh_i. The work extracted in the process is given by $W = g\sum_i m_i\Delta h_i$. The partition exhibits large fluctuations, but repetitions of the process allow for approximation of the ensemble average of the work. Clearly, the protocol can be refined by adding more steps with smaller masses, where quasistatic control will be achieved at the limit of infinitely many infinitesimally small masses.

In Fig. 5(b) we plot the upper bound of the extractable work $W(k)$ (solid green line), calculated for a quasistatic process, the expected work (see Appendix B) for the

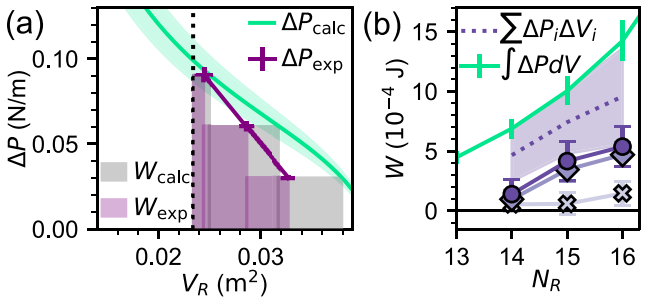

FIG. 5. Experimental and predicted work extraction for the three-step expansion protocol compared to the quasistatic limits. (a) Pressure difference applied on the partition as a function of the right half's volume V_R at $N_R/N = 15/17$. The calculated pressure difference ΔP on the partition, based on data from Fig. 2, is shown in a solid green line. The experimental results are shown in purple points. The initial volume is $V_R = V/2$, shown in a dotted vertical line. The work extracted at each step is $W = \Delta P \Delta V$ (area of gray and purple rectangles for calculated and experimental results, respectively). (b) Work extracted from the system for experiments with different values of N_R/N for $N = 17$ after one (crosses), two (diamonds), and three (circles) stages of the protocol. For $N_R = 15$, values correspond to the areas of purple rectangles in (a). Results are compared to the expected work from the finite-time protocol with three control steps (dashed purple line), and the optimal control protocol (solid green line).

three-stage protocol (dashed purple lines), and the measured work (markers) for experiments with $N = 17$ and $N_R = 14, 15, 16$. The measured work exhibits the same trends as its expected counterpart and also falls just within experimental uncertainty. However, it also is systematically smaller than expected. This difference is attributed to a mechanical constraint that restricts the maximally attainable volume (see Appendix B). Nevertheless, the results show that more work can be extracted when the imbalance between the number of particles in the two halves is larger, and as more control steps are added. This verifies that pressure measurements are reliable and can be used to calculate the amount of extracted work for a given work extraction protocol, hence demonstrating that work of order 10^{-4} J can be extracted from the engine, as predicted in Fig. 4.

IV. CONCLUSIONS

In summary, we report the first experimental study of a macroscopic information engine operating on an active system. Our implementation was based on a many-body Szilárd's engine configuration consisting of self-propelled bbots. We analyzed the operation of the engine in comparison to one based on an ideal gas. The differences between the two reveal themselves in the dependence of the work per cycle on the number of particles. Specifically, the extractable work increases with particle number in our active engine, while decreasing in an ideal gas engine. This fundamental difference is attributed to the giant number fluctuations exhibited by the active system. This is a general result and should hold for any system with giant number fluctuations and monotonous dependence of pressure on density. While previous studies of work extraction from active systems were based on the interaction between active matter and boundaries [56–60], here we use a different attribute of active matter: their tendency to aggregate.

In addition, we demonstrated how different protocols affect the extracted work. It would be interesting to explore different protocols to maximize work extraction at finite operation times, especially in light of the literature on optimal control of active matter [61–64]. Clearly, more work could be extracted from our system using more elaborated feedback and control schemes that employ information about the dynamics of the partition during the expansion process.

Fluctuations in our experiment are athermal and can occur at any scale, without the amplification required in Ref. [65]. This allowed us to extract work with an order of magnitude $\alpha \simeq 10^{-4}$ J per cycle, where α is the scaling factor between pressure and density for the bbots (Fig. 2). In comparison, state-of-the-art microscopic information engines can only extract up to about $k_B T \simeq 10^{-21}$ J per cycle [16,18], or $10 k_B T \simeq 10^{-20}$ J when a passive particle is subjected to nonequilibrium fluctuations [33,34]. Notably, the energy scale α in our experiment is also three orders of magnitude larger than that measured for a macroscopic Maxwell's demon operating on a granular gas [60].

To compare our results to microscopic information engines on equal footings, we also evaluate the normalized values of work and η_c. The ideal work per cycle (Fig. 4) is $\langle W \rangle/\alpha \simeq 3.88$ at $N = 25$, which is comparable to $\langle W \rangle/k_B T \simeq 1$ values in microscopic engines [16–18]. The corresponding maximum value of η_c we observed is $\eta_c = \langle W \rangle/\alpha I = 1.21 \pm 0.42$, which is of course a result of the energy required to maintain activity not being taken into account. A conversion efficiency $\eta_c > 1$ highlights the nonequilibrium dynamics the active particles. This is in line with the results of Ref. [33] but in stark contrast to the situation in Ref. [34], where the nonequilibrium fluctuations are analogous to thermal fluctuations at a high effective temperature.

Finally, we note that when considering the energy required to sustain the active system in a steady state, the full thermodynamic efficiency of our active information engine is naturally very low. This is a result of only a fraction of the total energy being used to push the partition. Evidently, directly connecting the batteries to an electric engine would yield a significantly higher power output than can be extracted from the movement of the partition. However, understanding the various mechanisms by which energy can be extracted from active matter is fundamentally interesting. It will also assist in the design of microscopic engines operating in naturally occurring active systems, such as bacteria swarms.

ACKNOWLEDGMENTS

We thank Isaac Yekotiel and the Chemistry Machine Shop of Tel Aviv University for the design and construction of the experimental system. O.C. and Y.R. acknowledge support from the European Research Council (ERC) under the European Union's Horizon 2020 research and innovation Program (Grant No. 101002392). A.S. and Y.R. acknowledge support from the Israel Science Foundation (Grant No. 385/21). S.R. is grateful for support from the Israel Science Foundation

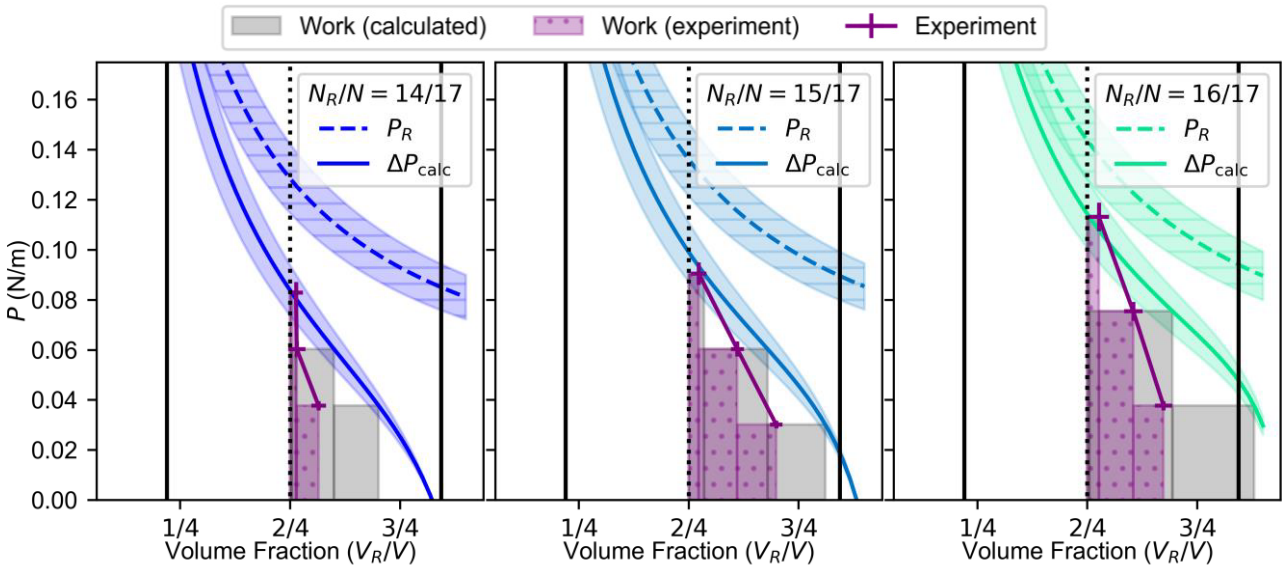

FIG. 6. Pressure-volume diagram for the system at different N_R/N ratios. The pressure difference $\Delta P = P_R - P_L$ between both sides as a function of the volume of the right side V_R is shown in a solid line. The pressure of the right side P_R is shown in a dashed line for comparison. The grey boxes are the expected work output for each control step used in the experiment [$P_i \Delta V_i$ in Eq. (B5)]. The purple lines and boxes show the actual mean volume at which the system equilibrated in the experiment and the corresponding real output work. The initial volume $V/2$ is shown in a dotted vertical line, whereas the maximum and minimum volumes are shown in solid black lines (the geometry of the system prevents the volume of the right half of the system from exceeding these values).

(Grant No. 1929/21). R.G. acknowledges support from the Ratner Center for Single Molecule sciences.

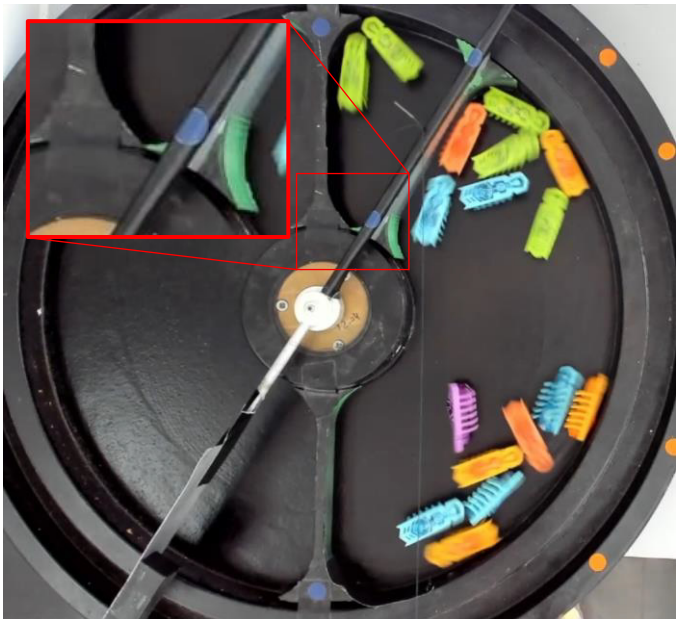

FIG. 7. This snapshot taken from one of the experiments illustrates that the volume distribution is truncated due to the geometry of the arena. Rounded corners prevent the side with more particles from expanding further, even though several particles are pushing against the partition and particles from the other side do not apply any force on the partition. Inset: a zoomed in picture of the corner that restricts the partition from moving further.

APPENDIX A: DEPENDENCE OF WORK ON NUMBER FLUCTUATIONS

Consider a system with N particles and volume V_{tot}, in which the pressure $P(\rho)$ is a monotonic function of the density ρ. A wall is placed in the center of the system, dividing it into two subsystems of volume $\frac{1}{2}V_{tot}$, with N_L and N_R particles in the left and right halves, respectively, so that $N_L + N_R = N$. We let the partition move due to the force applied to it by pressure difference on both sides, $\Delta P = P_R - P_L$, until a mechanical equilibrium state $P_R = P_L$ is reached. Due to the assumption on P, this occurs when the volume of each side reaches a value so that densities are equal:

$$\rho^{eq} = \frac{N_L}{V_L^{eq}} = \frac{N_R}{V_R^{eq}}. \tag{A1}$$

Define the volume difference ΔV between the initial and final volumes of each side so that $V_L^{eq} = V_{tot}/2 - \Delta V$ and $V_R^{eq} = V_{tot}/2 + \Delta V$. Also denote $N_L = N/2 - \Delta N$ and $N_R = N/2 + \Delta N$, then

$$\frac{1 - 2\Delta N/N}{1 + 2\Delta N/N} = \frac{1 - 2\Delta V/V_{tot}}{1 + 2\Delta V/V_{tot}}, \tag{A2}$$

$$\frac{\Delta N}{N} = \frac{\Delta V}{V_{tot}}, \tag{A3}$$

where N and V_{tot} are constants, so ΔV is a function of the random variable ΔN, whose value is determined when the wall is placed, dividing the full system into two subsystems. The work extracted from a quasistatic process is given by

$$W = \int_{\frac{V_{tot}}{2}}^{V_{eq}^R} \Delta P(V_R) dV_R \tag{A4}$$

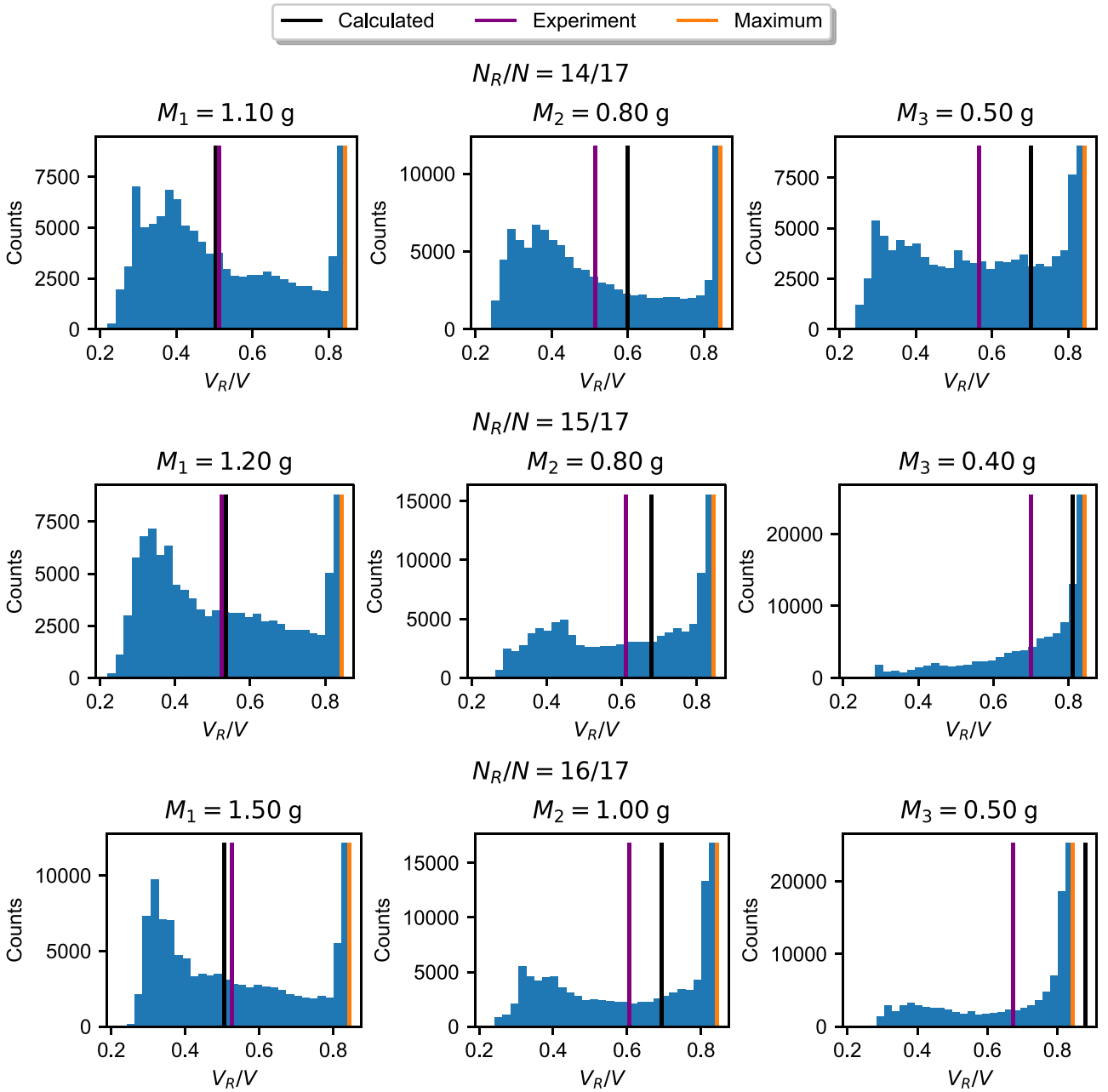

FIG. 8. Volume distribution experimentally measured for each N_R/N ratio at different applied weights. The measured volumes are shown in blue and their average is in a purple line. This is compared to the predicted volume from Eq. (B4) (solid black line). The maximum achievable volume (constrained by the geometry of the arena) is shown in orange. The increased counts near the maximum volume indicate that the distribution is indeed truncated at this value.

$$= \int_{\frac{V_{tot}}{2}}^{V_R^{eq}} P_R(\rho_R) dV_R - \int_{\frac{V_{tot}}{2}}^{V_R^{eq}} P_L(\rho_L) dV_R \qquad \text{(A5)}$$

$$= \int_{\frac{V_{tot}}{2}}^{V_R^{eq}} P_R(\rho_R) dV_R + \int_{\frac{V_{tot}}{2}}^{V_L^{eq}} P_L(\rho_L) dV_L. \qquad \text{(A6)}$$

Since the number of particles in each partition remains constant, we can substitute $V_i = N_i/\rho_i$ and $dV_i = -(N_i/\rho_i^2)d\rho_i$ ($i \in L, R$), so that

$$W = -N_R \int_{\frac{2N_R}{V_{tot}}}^{\rho^{eq}} \frac{P(\rho_R)}{\rho_R^2} d\rho_R - N_L \int_{\frac{2N_L}{V_{tot}}}^{\rho^{eq}} \frac{P(\rho_L)}{\rho_L^2} d\rho_L. \qquad \text{(A7)}$$

Since V_{tot} is a constant and N_L, N_R and ΔV are all functions of ΔN, we found that the work W can be recast as a function of ΔN, i.e., its mean and fluctuations can be calculated from the number fluctuations in the setup.

APPENDIX B: CALCULATIONS OF WORK IN THE DISCRETE CONTROL PROTOCOL

In the three-step expansion protocol, the system is initially divided into two halves of volume $V/2$ with $N_{L,R}$ particles at each half. Let us assume that a mass m is attached to the partition and calculate the volumes V_L, V_R at which mechanical

equilibrium is achieved. These satisfy

$$L\Delta P = mg, \tag{B1}$$

where L is the length of the partition, ΔP is the pressure difference between the two sides, and g is the gravity acceleration. Using the linear relation between density and pressure, shown in Fig. 2 of the main text, leads to

$$\alpha\frac{N_R}{V_R} - \frac{mg}{L} = \alpha\frac{N_L}{V_L}, \tag{B2}$$

$$\left(\alpha N_R - \frac{mg}{L}V_R\right)V = \left(\alpha(N_R+N_L) - \frac{mg}{L}V_R\right)V_R. \tag{B3}$$

We solve the quadratic equation for V_R

$$V_R(m,N_R,N_L) = \frac{1}{2}\Bigg(V + \frac{\alpha L}{mg}(N_R+N_L) \pm \sqrt{\left(\frac{\alpha L}{mg}(N_R+N_L)+V\right)^2 - 4\frac{\alpha L}{mg}N_R V}\Bigg) \tag{B4}$$

and since V_R should grow with N_R for fixed $N = N_R + N_L$, only the solution with the minus sign is physical.

The mechanical equilibrium value of V_R can be used to compute the extracted work for a protocol consisting of n masses m_i: define $M_i = \sum_{j=i}^{n} m_j$ the total mass at step i (beginning with a heavy total mass and gradually reducing the mass by removing some of the weights), the extracted work is

$$W = \sum_i P_i \Delta V_i = \sum_{i=1}^{n-1} \frac{M_i g}{L}\left(V_R(M_i,N_R,N_L) - V_R(M_{i-1},N_R,N_L)\right), \tag{B5}$$

with M_0 defined so that $V_R(M_0,N_R,N_L) = V/2$ (the initial volume is one half of the arena for any protocol).

In Fig. 6, we plot the expected extracted work for the masses used in the experiment for several N_R/N ratios [Eq. (B5)], and compare the calculations to experimentally measured values. The figure illustrates how adding more control steps allows the extracted work to approach its quasistatic limit.

Deviation of the experimental work from its predicted values. Our results, see for example Fig. 6, show that while for a larger mass, the mean volume the system is found at is consistent with the prediction based on pressure measurements, as the mass is reduced a deviation from the predicted value observed. We suggest that this is mainly a result of the truncation of the volume distribution caused by the geometry of the arena. Figure 7 shows a snapshot from an experiment where the partition cannot move despite being pushed by particles only from one side. The inset shows it is the rounded corners that prevent the setup from reaching very large volumes. This is supported further by observing the volume distributions for different N_R/N ratios and different applied weights. Figure 8 shows the measured distributions for all the measurements contributing to the data presented in Fig. 6. Clearly, the distributions in all experiments are affected by this restriction, as they all show an increased likelihood to be at the cutoff volume, and absence of larger volumes. But for larger masses, only realizations near the tail of the distribution are affected, and their overall weight is relatively small. Indeed, for these masses, the observed mean volume matches the calculated value. When the mass of the weight is reduced the distribution of volumes is shifted towards larger values. As a result, more realizations are found at the cutoff volume, meaning that the truncation effect is more prominent. This explains why the experimental extracted work agrees with its predicted value based on pressure measurements in the first control step, where the applied mass is very large (so only a small pressure imbalance is expected), and deviates more as the weight is decreased (a larger imbalance should result in V_R expanding further towards its maximal value).

This observation explains the systematic deviations between the measured work and the results of calculations based on Eq. (B4). Indeed, one can see in Fig. 6 that much of the discrepancy comes from the latter stages of the process, where the weights are smaller, and volumes are typically larger. An improved theoretical calculation that would take into account the cutoff will require a description of the distribution of volume and is unrealistic. In a larger experimental setup that would minimize finite-size effects we expect better agreement between calculated and measured work.

[1] J. M. Parrondo, J. M. Horowitz, and T. Sagawa, Thermodynamics of information, Nat. Phys. **11**, 131 (2015).

[2] R. Landauer, Irreversibility and heat generation in the computing process, IBM J. Res. Dev. **5**, 183 (1961).

[3] C. H. Bennett, Logical reversibility of computation, IBM J. Res. Dev. **17**, 525 (1973).

[4] T. Sagawa and M. Ueda, Second law of thermodynamics with discrete quantum feedback control, Phys. Rev. Lett. **100**, 080403 (2008).

[5] F. J. Cao and M. Feito, Thermodynamics of feedback controlled systems, Phys. Rev. E **79**, 041118 (2009).

[6] J. M. Horowitz and S. Vaikuntanathan, Nonequilibrium detailed fluctuation theorem for repeated discrete feedback, Phys. Rev. E **82**, 061120 (2010).

[7] T. Sagawa and M. Ueda, Generalized Jarzynski equality under nonequilibrium feedback control, Phys. Rev. Lett. **104**, 090602 (2010).

[8] M. Ponmurugan, Generalized detailed fluctuation theorem under nonequilibrium feedback control, Phys. Rev. E **82**, 031129 (2010).

[9] Y. Fujitani and H. Suzuki, Jarzynski equality modified in the linear feedback system, J. Phys. Soc. Jpn. **79**, 104003 (2010).

[10] A. Kundu, Nonequilibrium fluctuation theorem for systems under discrete and continuous feedback control, Phys. Rev. E **86**, 021107 (2012).

[11] J. C. Maxwell, *Theory of heat* (Longmans, Green, & Co., London, UK, 1871).

[12] T. Admon, S. Rahav, and Y. Roichman, Experimental realization of an information machine with tunable temporal correlations, Phys. Rev. Lett. **121**, 180601 (2018).

[13] Y. Jun, M. Gavrilov, and J. Bechhoefer, High-precision test of Landauer's principle in a feedback trap, Phys. Rev. Lett. **113**, 190601 (2014).

[14] A. Bérut, A. Arakelyan, A. Petrosyan, S. Ciliberto, R. Dillenschneider, and E. Lutz, Experimental verification of Landauer's principle linking information and thermodynamics, Nature (London) **483**, 187 (2012).

[15] S. Toyabe, T. Sagawa, M. Ueda, E. Muneyuki, and M. Sano, Experimental demonstration of information-to-energy conversion and validation of the generalized Jarzynski equality, Nat. Phys. **6**, 988 (2010).

[16] M. Ribezzi-Crivellari and F. Ritort, Large work extraction and the Landauer limit in a continuous Maxwell demon, Nat. Phys. **15**, 660 (2019).

[17] G. Paneru, D. Y. Lee, T. Tlusty, and H. K. Pak, Lossless Brownian information engine, Phys. Rev. Lett. **120**, 020601 (2018).

[18] T. K. Saha, J. N. Lucero, J. Ehrich, D. A. Sivak, and J. Bechhoefer, Maximizing power and velocity of an information engine, Proc. Natl. Acad. Sci. USA **118**, e2023356118 (2021).

[19] G. Paneru and H. Kyu Pak, Colloidal engines for innovative tests of information thermodynamics, Adv. Phys.: X **5**, 1823880 (2020).

[20] J. V. Koski, V. F. Maisi, T. Sagawa, and J. P. Pekola, Experimental observation of the role of mutual information in the nonequilibrium dynamics of a Maxwell demon, Phys. Rev. Lett. **113**, 030601 (2014).

[21] J. V. Koski, V. F. Maisi, J. P. Pekola, and D. V. Averin, Experimental realization of a Szilard engine with a single electron, Proc. Natl. Acad. Sci. USA **111**, 13786 (2014).

[22] Y. Masuyama, K. Funo, Y. Murashita, A. Noguchi, S. Kono, Y. Tabuchi, R. Yamazaki, M. Ueda, and Y. Nakamura, Information-to-work conversion by Maxwell's demon in a superconducting circuit quantum electrodynamical system, Nat. Commun. **9**, 1291 (2018).

[23] N. Cottet, S. Jezouin, L. Bretheau, P. Campagne-Ibarcq, Q. Ficheux, J. Anders, A. Auffèves, R. Azouit, P. Rouchon, and B. Huard, Observing a quantum Maxwell demon at work, Proc. Natl. Acad. Sci. USA **114**, 7561 (2017).

[24] M. D. Vidrighin, O. Dahlsten, M. Barbieri, M. S. Kim, V. Vedral, and I. A. Walmsley, Photonic Maxwell's demon, Phys. Rev. Lett. **116**, 050401 (2016).

[25] L. Szilard, Über die entropieverminderung in einem thermodynamischen system bei eingriffen intelligenter wesen, Z. Phys. **53**, 840 (1929).

[26] K. H. Kim and S. W. Kim, Information from time-forward and time-backward processes in Szilard engines, Phys. Rev. E **84**, 012101 (2011).

[27] J. M. Horowitz and J. M. Parrondo, Designing optimal discrete-feedback thermodynamic engines, New J. Phys. **13**, 123019 (2011).

[28] J. Song, S. Still, R. Diaz Hernandez Rojas, I. Perez Castillo, and M. Marsili, Optimal work extraction and mutual information in a generalized Szilárd engine, Phys. Rev. E **103**, 052121 (2021).

[29] S. W. Kim, T. Sagawa, S. De Liberato, and M. Ueda, Quantum Szilard engine, Phys. Rev. Lett. **106**, 070401 (2011).

[30] J. Bengtsson, M. N. Tengstrand, A. Wacker, P. Samuelsson, M. Ueda, H. Linke, and S. M. Reimann, Quantum Szilard engine with attractively interacting bosons, Phys. Rev. Lett. **120**, 100601 (2018).

[31] C. Y. Cai, H. Dong, and C. P. Sun, Multiparticle quantum Szilard engine with optimal cycles assisted by a Maxwell's demon, Phys. Rev. E **85**, 031114 (2012).

[32] H. J. Jeon and S. W. Kim, Optimal work of the quantum Szilard engine under isothermal processes with inevitable irreversibility, New J. Phys. **18**, 043002 (2016).

[33] T. K. Saha, J. Ehrich, M. Gavrilov, S. Still, D. A. Sivak, and J. Bechhoefer, Information engine in a nonequilibrium bath, Phys. Rev. Lett. **131**, 057101 (2023).

[34] G. Paneru, S. Dutta, and H. K. Pak, Colossal power extraction from active cyclic Brownian information engines, J. Phys. Chem. Lett. **13**, 6912 (2022).

[35] P. Malgaretti and H. Stark, Szilard engines and information-based work extraction for active systems, Phys. Rev. Lett. **129**, 228005 (2022).

[36] I. Goldhirsch and G. Zanetti, Clustering instability in dissipative gases, Phys. Rev. Lett. **70**, 1619 (1993).

[37] V. Narayan, S. Ramaswamy, and N. Menon, Long-lived giant number fluctuations in a swarming granular nematic, Science **317**, 105 (2007).

[38] J. Deseigne, O. Dauchot, and H. Chaté, Collective motion of vibrated polar disks, Phys. Rev. Lett. **105**, 098001 (2010).

[39] S. Ramaswamy, R. A. Simha, and J. Toner, Active nematics on a substrate: Giant number fluctuations and long-time tails, Europhys. Lett. **62**, 196 (2003).

[40] J. Toner, Y. Tu, and S. Ramaswamy, Hydrodynamics and phases of flocks, Ann. Phys. **318**, 170 (2005).

[41] F. Ginelli, F. Peruani, M. Bär, and H. Chaté, Large-scale collective properties of self-propelled rods, Phys. Rev. Lett. **104**, 184502 (2010).

[42] H. Chaté, F. Ginelli, G. Grégoire, and F. Raynaud, Collective motion of self-propelled particles interacting without cohesion, Phys. Rev. E **77**, 046113 (2008).

[43] H.-P. Zhang, A. Be'er, E.-L. Florin, and H. L. Swinney, Collective motion and density fluctuations in bacterial colonies, Proc. Natl. Acad. Sci. USA **107**, 13626 (2010).

[44] J. Palacci, S. Sacanna, A. P. Steinberg, D. J. Pine, and P. M. Chaikin, Living crystals of light-activated colloidal surfers, Science **339**, 936 (2013).

[45] A. Bricard, J.-B. Caussin, N. Desreumaux, O. Dauchot, and D. Bartolo, Emergence of macroscopic directed motion in populations of motile colloids, Nature (London) **503**, 95 (2013).

[46] See Supplemental Material at http://link.aps.org/supplemental/10.1103/PhysRevResearch.5.043193 for movies of the experimental setup, pressure measurements, and work extraction.

[47] L. Giomi, N. Hawley-Weld, and L. Mahadevan, Swarming, swirling and stasis in sequestered bristle-bots, Proc. R. Soc. A **469**, 20120637 (2013).

[48] A. Deblais, T. Barois, T. Guerin, P.-H. Delville, R. Vaudaine, J. S. Lintuvuori, J.-F. Boudet, J.-C. Baret, and H. Kellay, Boundaries control collective dynamics of inertial self-propelled robots, Phys. Rev. Lett. **120**, 188002 (2018).

[49] R. Sánchez and P. Díaz-Leyva, Self-assembly and speed distributions of active granular particles, Phys. A **499**, 11 (2018).

[50] O. Dauchot and V. Démery, Dynamics of a self-propelled particle in a harmonic trap, Phys. Rev. Lett. **122**, 068002 (2019).

[51] X. Yang, M. L. Manning, and M. C. Marchetti, Aggregation and segregation of confined active particles, Soft Matter **10**, 6477 (2014).

[52] S. C. Takatori, W. Yan, and J. F. Brady, Swim pressure: stress generation in active matter, Phys. Rev. Lett. **113**, 028103 (2014).

[53] G. Bradski, The OpenCV library, Dr. Dobb's Journal: Software Tools **25**, 120 (2000).

[54] J.-M. Park, J. S. Lee, and J. D. Noh, Optimal tuning of a confined Brownian information engine, Phys. Rev. E **93**, 032146 (2016).

[55] B. Andresen, R. S. Berry, A. Nitzan, and P. Salamon, Thermodynamics in finite time. I. The step-Carnot cycle, Phys. Rev. A **15**, 2086 (1977).

[56] Y. Hiratsuka, M. Miyata, T. Tada, and T. Q. Uyeda, A microrotary motor powered by bacteria, Proc. Natl. Acad. Sci. USA **103**, 13618 (2006).

[57] L. Angelani, R. Di Leonardo, and G. Ruocco, Self-starting micromotors in a bacterial bath, Phys. Rev. Lett. **102**, 048104 (2009).

[58] R. Di Leonardo, L. Angelani, D. Dell'Arciprete, G. Ruocco, V. Iebba, S. Schippa, M. P. Conte, F. Mecarini, F. De Angelis, and E. Di Fabrizio, Bacterial ratchet motors, Proc. Natl. Acad. Sci. USA **107**, 9541 (2010).

[59] L. Angelani, A. Costanzo, and R. Di Leonardo, Active ratchets, Europhys. Lett. **96**, 68002 (2011).

[60] M. Lagoin, C. Crauste-Thibierge, and A. Naert, Human-scale Brownian ratchet: A historical thought experiment, Phys. Rev. Lett. **129**, 120606 (2022).

[61] D. Gupta, S. H. Klapp, and D. A. Sivak, Efficient control protocols for an active Ornstein-Uhlenbeck particle, Phys. Rev. E **108**, 024117 (2023).

[62] M. M. Norton, P. Grover, M. F. Hagan, and S. Fraden, Optimal control of active nematics, Phys. Rev. Lett. **125**, 178005 (2020).

[63] S. Shankar, V. Raju, and L. Mahadevan, Optimal transport and control of active drops, Proc. Natl. Acad. Sci. USA **119**, e2121985119 (2022).

[64] Y. Yang and M. A. Bevan, Optimal navigation of self-propelled colloids, ACS Nano **12**, 10712 (2018).

[65] N. Freitas and M. Esposito, Maxwell demon that can work at macroscopic scales, Phys. Rev. Lett. **129**, 120602 (2022).